

UDK: 532.74; 666.3.019; 622.785

Morphological and Structural Characterization of MgAl₂O₄ Spinel

Nina Obradović^{1*}, Suzana Filipović¹, William G. Fahrenholtz², Bojan A. Marinković³, Jelena Rogan⁴, Steva Lević⁵, Antonije Đorđević⁶, Vladimir B. Pavlović⁵

¹Institute of Technical Sciences of the Serbian Academy of Sciences and Arts, 11000 Belgrade, Serbia

²Materials Science and Engineering, Missouri University of Science and Technology, Rolla, Missouri, United States

³Departamento de Engenharia Química e de Materiais, Pontifícia Universidade Católica do Rio de Janeiro, Rio de Janeiro, Brazil

⁴Department of General and Inorganic Chemistry, Faculty of Technology and Metallurgy, University of Belgrade, 11120 Belgrade, Serbia

⁵Faculty of Agriculture, University of Belgrade, 11000 Belgrade, Serbia

⁶Serbian Academy of Sciences and Arts, 11000 Belgrade, Serbia

Abstract:

Magnesium aluminate has the spinel structure along with good mechanical, chemical, and thermal properties. Magnesium aluminate has a wide range of applications including refractory ceramics, optically transparent ceramic windows, and armors. Its low dielectric permeability and low loss tangent enable its applications for integrated electronic devices, as well. In this paper, MgO and Al₂O₃ powders were mixed in a one-to-one molar ratio and calcined at temperatures ranging from 1500 to 1800°C to produce phase pure spinel. Thereafter, pellets were crushed and treated in a planetary ball mill for 60 min to obtain a fine powder. All powders were examined for phase composition, crystal structure, and morphology. The obtained results showed that by increasing the temperature, samples with higher density were synthesized. Milling for 1 h led to formation of larger particles, but finer powders after milling. XRPD and Raman spectroscopy showed disorder in the crystal structure after milling.

Keywords: Spinel; Mechanical activation; Sintering; Structure.

1. Introduction

Magnesium aluminate spinel (MAS) is a material of great importance owing to its high melting point (> 2100°C), and excellent mechanical and thermal properties, low dielectric constant (~ 8), and loss tangent [1]. MAS possesses high chemical resistance as well as good radiation resistance [2]. These properties make MAS a candidate for a wide range of applications. It can be successfully used as a dense ceramic or as a porous one. As the dense ceramic, the most common applications are as refractory ceramics and in electronic devices [3–6]. Fully dense MgAl₂O₄ can be transparent and applied for manufacturing transparent

*) **Corresponding author:** nina.obradovic@itn.sanu.ac.rs (Dr. Nina Obradović)

armors or IR windows [7–9]. On the other hand, porous MAS ceramics are usually used as humidity sensors and catalysts [10, 11]. Recently, interest has increased for use of this material as a filter for wastewater purification owing to its high adsorption capacity [12, 13].

The general formula of spinel type of compounds is AB_2O_4 , where A is a divalent and B is a trivalent cation. $MgAl_2O_4$ belongs to the space group $Fd\bar{3}m$ (227). The cubic structure contains a closed packed array of 32 oxygen atoms and has cations in both octahedral and tetrahedral positions. In a normal spinel-like structure, 8 divalent cations (Mg^{2+}) are in the tetrahedral sites and 16 trivalent cations (Al^{3+}) are in the octahedral sites. Due to similar cation radii, Mg can occupy some octahedral sites and Al atoms can occupy some tetrahedral sites, a process that is called inversion [14–16]. The exchange between Mg^{2+} and Al^{3+} cations occurs with increasing temperature or pressure. That obtained disorder, usually called intrinsic anti-site disorder, leads to formation of partially inverse spinel. MAS spinel was found to have a high interstitial-vacancy (i–v) recombination rate and the ability of the lattice to tolerate significant intrinsic anti-site disorder on the cation sub-lattice. This is especially important for usage in cores for fusion reactors.

The influence of mechanical activation on synthesis of MAS through two heating steps along with changes in the crystal lattice and inversion process were investigated using scanning electron microscopy (SEM), energy dispersive x-ray spectroscopy (EDS), powder x-ray diffraction (XRPD), and Raman spectroscopy.

2. Materials and Experimental Procedures

Magnesium oxide powder ($\geq 99\%$, Sigma-Aldrich, p.a.) was calcined in air at 1000°C for 1 h at a heating rate of $10^\circ\text{C}\cdot\text{min}^{-1}$ to remove hydroxide and carbonate species. The as-calcined MgO powder was mixed with alumina powder ($\geq 99\%$, Sigma-Aldrich, p.a.) via dry-ball milling for 24 h with alumina media. A media-to-powder weight ratio of 1:1 was used. After mixing, the precursor powder was ground and sieved to 80 mesh. The precursor powder was reacted in air at temperatures of 1500, 1600, 1700, and 1800°C . The heating rate was $10^\circ\text{C}\cdot\text{min}^{-1}$ with 1 h holding time. The as-obtained samples were denoted according to applied temperatures as MAS1500K–MAS1800K. The reacted powders were then ground and sieved to 80 mesh. Powders were pressed into pellets under a uniaxial pressure of 31 MPa. The pellets were reacted a second time at 1500, 1600, 1700, and 1800°C for 1 h, respectively. The pellets were crushed and then subjected to additional milling in a planetary ball mill for 60 min (Planetary Ball Mill Retsch PM 100, in air, using Y-stabilized ZrO_2 vials and balls 5 mm in diameter). Ball-to-powder ratio was 30:1. After the milling process, the prepared samples were labeled as MAS1500M–MAS1800M.

Sintered specimens were subjected to X-Ray powder diffraction (X'Pert Pro, PANalytical, Almelo, NLD). Phase analysis was performed by Rietveld refinement (RIQAS4, Materials Data Incorporated, Livermore, USA). Lattice parameters determined using Rietveld refinement of XRD data were used to calculate the theoretical density of sintered bodies, assuming cubic crystal structure and the space group $Fd\bar{3}m$ (227). Microstructure was examined by scanning electron microscopy (JEOL JSM-6390 LV). The samples were coated with a conductive Au coating before placing into the SEM. Raman spectra were recorded in the $200\text{--}900\text{ cm}^{-1}$ range using an XploRA Raman spectrometer from Horiba Jobin–Yvon, with a 532 nm laser at a maximum output power of 20–25 mW. To prevent damage by the laser, power was reduced using a 10% filter. All measurements were realized using a spectrometer equipped with a grating that had $2400\text{ lines}\cdot\text{mm}^{-1}$ and 5 acquisition cycles with a 10 s acquisition time. A 50x microscope objective and long working distance were used for laser focusing.

3. Results and Discussion

XRPD patterns of calcined samples are presented in Fig. 1a. All detected peaks were sharp and intense, indicating high crystallinity with large coherently diffracting domains. Magnesium aluminate was the only phase detected in all calcined specimens. Rietveld analysis corroborated the presence of phase pure spinel in all sintered specimens, with a crystallographic density of $3.584 \text{ g}\cdot\text{cm}^{-3}$, which corresponds to its theoretical value. Rietveld refinement data, shown in Table I, indicated an increase in lattice parameter and crystallite size with increasing calcination temperature. At the same time, strain values continuously decreased with temperature, indicating relaxation of the crystal lattice.

XRPD patterns of the mechanically activated samples are shown in Fig. 1b. Decreased intensity along with broadening was clearly observed for all peaks. The presence of trace amounts of alumina and MgO were noticed within MAS1500M. All peaks were identified using PDF cards 01-077-1203 for spinel, 45-0946 for MgO, and 74-1081 for alumina. Significant increase in strain values was detected in the activated powders compared to calcined powders, which was higher by almost one order of magnitude. This behavior was due to the increase in concentration of point defects (vacancies, interstitial atoms, and impurity atoms), line defects (atom aggregations on the crystal surface), or volume defects (pores and impurities), caused by the intense mechanical activation. In comparison with calcined specimens, the mechanically activated powders had increased the lattice parameter, crystallite size, and strain.

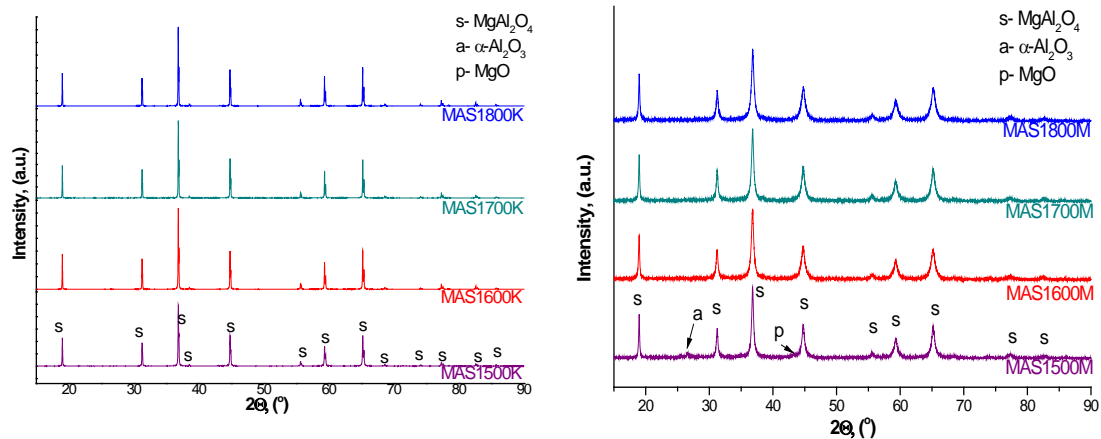


Fig. 1. XRD patterns of: a) calcined and b) ball-milled specimens.

Tab. I Structural parameters obtained by Rietveld analysis.

Sample	Crystal lattice parameter a (Å)	Mean crystallite size (nm)	Strain
MAS1500K	8.0872(4)	271(3)	0.0305(3)
MAS1600K	8.0876(3)	566(1)	0.0260(2)
MAS1700K	8.0874(3)	892(3)	0.0243(2)
MAS1800K	8.0887(4)	2030(8)	0.0272(2)
MAS1500M	8.0915(3)	2100(1)	0.0663(5)
MAS1600M	8.0911(3)	1740(1)	0.108(4)
MAS1700M	8.0907(3)	1860(1)	0.093(4)
MAS1800M	8.0913(3)	1650(1)	0.145(3)

SEM and EDS of powders after calcination are shown in Fig. 2. The sample heated to 1500°C consisted of particles between 300 and 600 nm with agglomerates around 3 μm in size. Larger agglomerates occurred with increasing the calcining temperature. Due to increase in mass transport, 3 to 7 μm sized agglomerates were observed. EDS images show uniform distribution of elements in the particles. The process of spinel formation was completed in all samples. As calcination temperature was raised, elemental homogeneity increased.

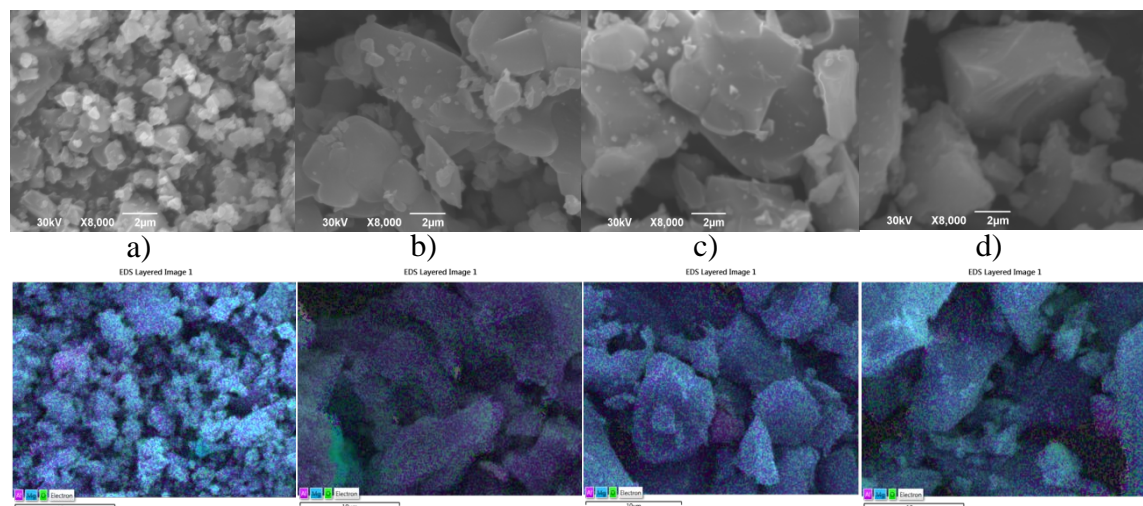


Fig. 2. SEM and EDS images of calcined specimens: a) MAS1500K, b) MAS1600K, c) MAS1700K, and d) MAS1800K.

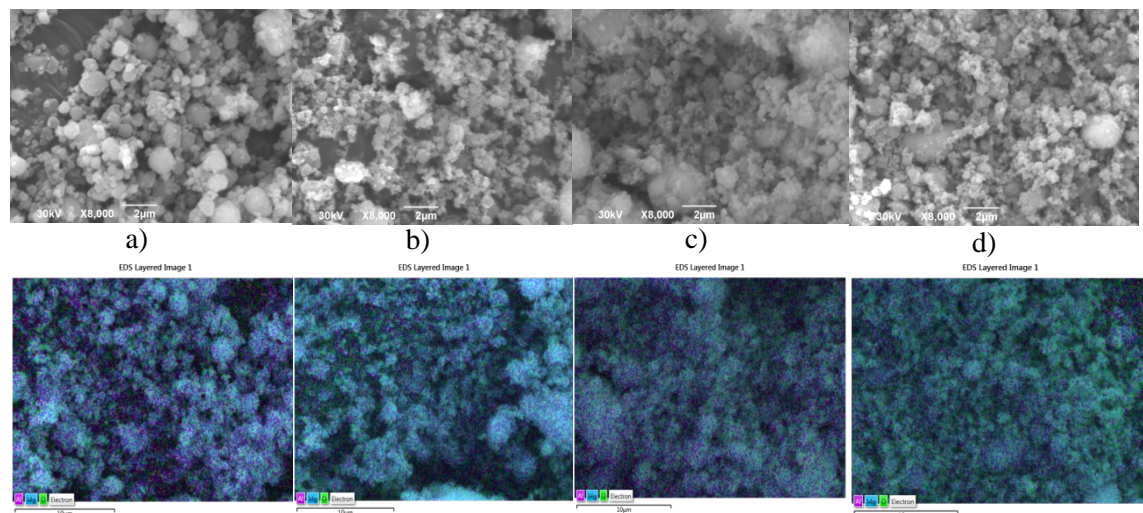


Fig. 3. SEM and EDS images of milled specimens: a) MAS1500M, b) MAS1600M, c) MAS1700M, and d) MAS1800M.

Microstructures of mechanically activated powders produced from crushed pellets are presented in Fig. 3. Significant fragmentation was observed. Milling in a planetary ball mill for one hour led to a decrease in particle size to around 200 nm. Two kinds of agglomerates were observed. Soft agglomerates were made up of small particles. Hard agglomerates, which were the consequence of previous heating treatment, had dimensions between 2 and 3 μm . Finer and more uniform microstructure without large and hard agglomerates is due to the process of mechanical activation [17, 18].

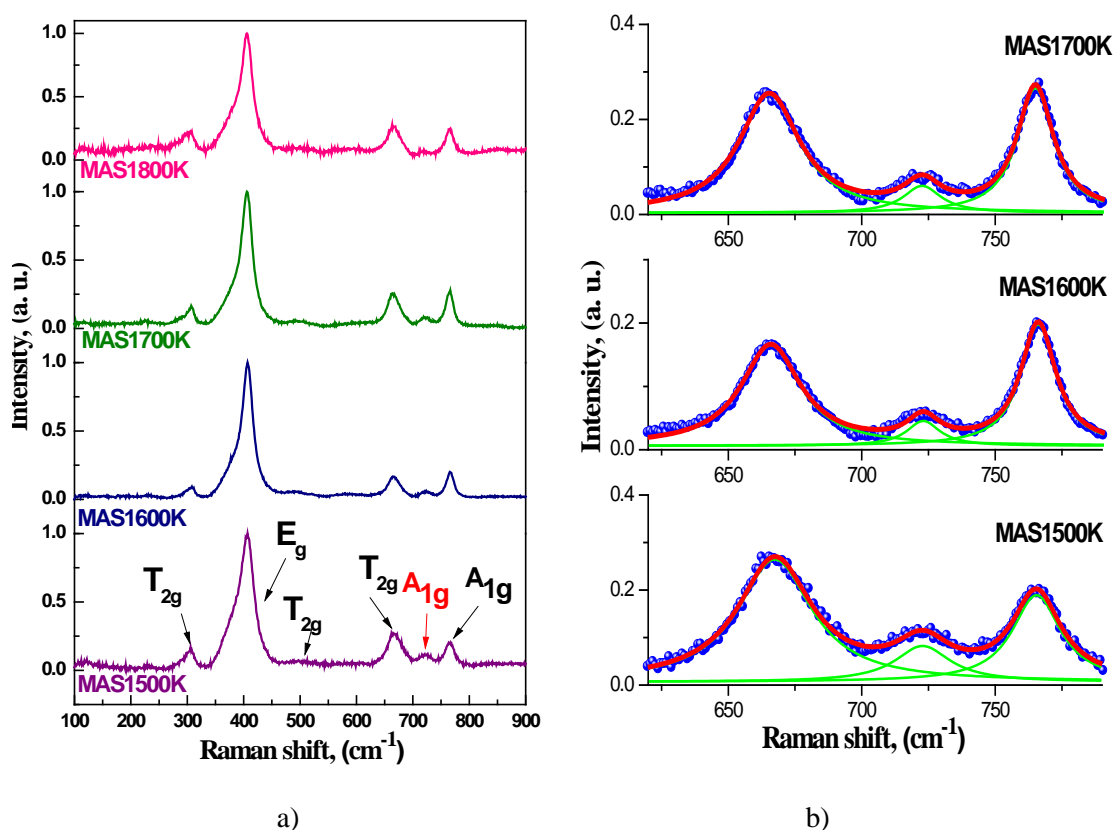


Fig. 4. Raman spectra for calcined specimens: (a) and (b) deconvolution of Raman spectra (green lines: separated Lorentzian peaks, red line: sum of Lorentzian peaks, blue circles measured data).

Raman spectra of calcined specimens are presented in Fig. 4a. Spinel MgAl_2O_4 belongs to the space group $Fd\bar{3}m$ (227) and exhibits five Raman active modes ($A_{1g} + E_g + 3T_{2g}$) [19, 20]. All five Raman active modes were observed, and their positions and intensity ratios were in good agreement with literature data [20]. In the normal spinel, only two sharp and well-defined peaks should be present above 600 cm^{-1} , while inverse spinel exhibits an additional A_{1g} peak appears at about 723 cm^{-1} [21, 22]. The presence of this additional peak was observed in all Raman spectra in the present study, indicating the existence of anti-site disorder the calcined samples. The lowest intensity of this peak was detected for the specimen calcined at 1800°C , while the intensity of the A_{1g} peak increased with decreasing calcination temperature. The results suggest an increase in the degree of disorder as calcination temperature decreases. The effects of calcination temperature were investigated in more detail by deconvolution the Raman spectra. Peaks in the range $630\text{--}800\text{ cm}^{-1}$ were fit to individual Lorentzian peaks as shown in Fig. 4b. Due to very low intensity of the A_{1g} peak, a deconvolution spectrum for MAS1800K was omitted. The mode at approx. 723 cm^{-1} had the same symmetry as the mode at approx. 770 cm^{-1} [23]. The peak at $\sim 723\text{ cm}^{-1}$ has been identified as a breathing mode of AlO_4 tetrahedral, which is connected to the presence of cationic disorder. Contrary to that, the peak at $\sim 770\text{ cm}^{-1}$ has been identified as symmetric stretching of $\text{Mg}\text{--}\text{O}$ bonds in MgO_4 tetrahedral, which is correlated to an ordered structure. Therefore, the intensity ratio of these separated Lorentzian peaks can be used as a measure of disorder in spinel MgAl_2O_4 [24].

Raman spectra of the milled specimens are presented in Fig. 5a. The presence of all five active Raman modes were visible. The additional A_{1g} peak was weaker than for the

calcined specimens, indicating a decreased degree of disorder. With milling, a Raman mode for α -alumina was observed. Considering that the most intense mode of spinel, at 410 cm^{-1} , had noticeable width, some of the alumina modes could be covered by this intense mode. Also, the modes of alumina have very similar position to the modes of spinel, so it is difficult to detect small amounts of alumina in spinel. A detailed analysis and deconvolution of Raman spectra were consistent with the presence of a small quantity of alumina. The peaks in the range $630\text{--}800\text{ cm}^{-1}$ were fit to individual Lorentzian peaks as shown in Fig. 5b.

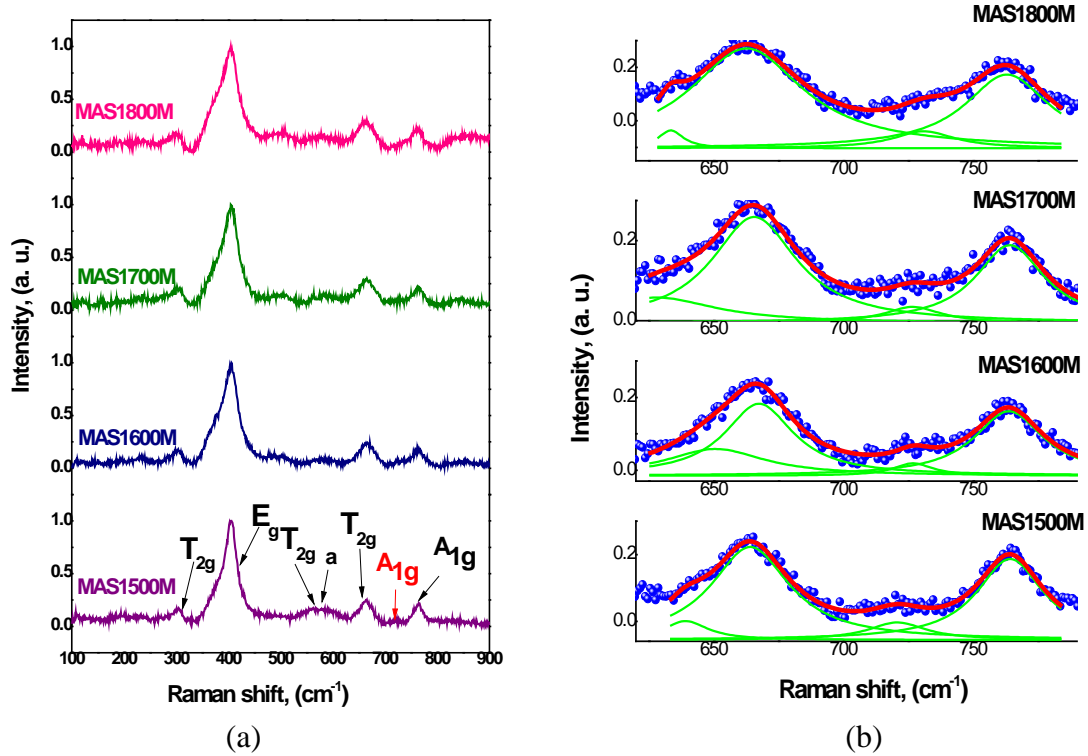


Fig. 5. Raman spectra for ball-milled specimens: (a) and (b) deconvolution of Raman spectra (green lines: separated Lorentzian peaks, red line: sum of Lorentzian peaks, blue circles measured data).

The inversion parameter can be calculated based on deconvolution of the Raman spectra using the equation [25]:

$$i = \frac{I_{dis}}{I_{dis} + I_{ord}} \quad (1)$$

where: I_{dis} and I_{ord} are intensities of the disordered and ordered modes, respectively. The inversion parameter was calculated as a function of temperature for both the calcined and milled samples as shown in Fig. 6. Inversion parameter decreased with increasing temperature of calcination. This behavior can be associated with annihilation of defects at elevated temperatures. With increasing the temperature from 1500 to 1600°C , the inversion parameter decreased significantly, and thereafter remained almost unchanged. The lattice parameter a vs. inversion parameter for the calcined and ball-milled specimens are presented in Fig. 7.

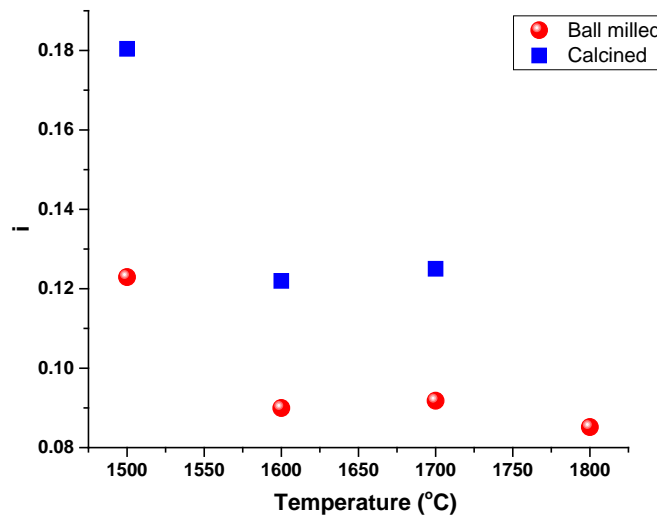


Fig. 6. Inversion parameter vs. temperature for calcined specimens and ball-milled specimens.

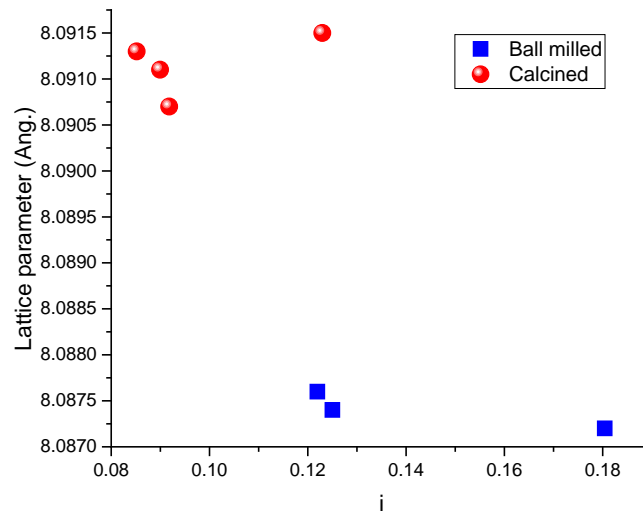


Fig. 7. Lattice parameter a vs. inversion parameter.

Literature data predicted the lattice parameter as a function of the cation disorder in MgAl_2O_4 spinel, using computer simulations, showed a relation between lattice parameter and inversion parameter [26]. These calculations showed that with increasing the inversion parameter, the lattice parameter decreased, which is in good agreement with our results presented in Fig. 7. In addition, an interesting phenomenon occurs here. The milled powders have smaller inversion parameters, suggesting lower level of anti-site disorder.

Previous studies report inversion parameters for natural spinel between 0.025 and 0.12, which is close to the results obtained for ball-milled samples. The lattice parameter a of the natural spinel is 8.0890 Å, while for our ball-milled specimens it was around 8.0910 Å [26].

4. Conclusion

The influence of mechanical activation was studied on the synthesis of MgAl_2O_4 spinel and its final properties. The focus was to monitor the influence of the 60-minute mechanical activation on morphology and structure of MAS powders. The main conclusions are:

- All specimens were nominally phase pure spinel after calcination, while milled specimens had some small content of alumina and magnesium oxide. The milled powders were more chemically homogeneous and with smaller uniform particles, without hard and large agglomerates.
- Along with all characteristic peaks that correspond to the spinel-type structure, an additional A_{1g} peak appeared at about 723 cm^{-1} , indicating the existence of anti-site disorder in the calcined samples. The mechanically activated samples exhibited lower A_{1g} peak, due to decreased degree of disorder.
- The inversion parameter was approximately 0.15 with the average lattice parameter a of 8.0876 \AA for calcined samples, while the mechanical activation decreased the inversion parameter to less than 0.10, increased the lattice parameter a to 8.0910 \AA , and lead to the structure close to natural-like spinel.

Acknowledgments

This work was financially supported by the Ministry of Science, Technological Development and Innovation of the Republic of Serbia (Contract Numbers 451-03-47/2023-01/200175, 451-03-68/2022-14/200116 and 451-03-9/2022-14/200135). The paper was written while Dr. Nina Obradović was a visiting scholar at Missouri University of Science and Technology, USA.

5. References

1. A. Zegadi, M. Kolli, M. Hamidouche, G. Fantozzi, Transparent MgAl_2O_4 spinel fabricated by spark plasma sintering from commercial powders, *Ceramics International* 44 (2018) 18828–18835.
2. Chenguang Liu, Yuhong Li, Tan Shi, Qing Peng, Fei Gao, Oxygen defects stabilize the crystal structure of MgAl_2O_4 spinel under irradiation, *Journal of Nuclear Materials* 527 (2019) 151830.
3. Wangding Peng, Zhe Chen, Wen Yan, Stefan Schafföner, Guangqiang Li, Yawei Li, Cangjian Jia, Advanced lightweight periclase-magnesium aluminate spinel refractories with high mechanical properties and high corrosion resistance, *Construction and Building Materials* 291 (2021) 123388.
4. Wenying Zhou, Wen Yan, Sanbao Ma, Stefan Schafföner, Yajie Dai, Yawei Li, Degradation mechanisms of periclase-magnesium aluminate spinel refractory bricks used in the upper transition zone of a cement rotary kiln, *Construction and Building Materials* 272 (2021) 121617.
5. Eduard Feldbach, Irina Kudryavtseva, Kenichiro Mizohata, Gatis Prieditis, Jyrki Räisänen, Evgeni Shablonin, Aleksandr Lushchik, Optical characteristics of virgin and proton-irradiated ceramics of magnesium aluminate spinel, *Optical Materials* 96 (2019) 109308.
6. V. Seeman, E. Feldbach, T. Kärner, A. Maaros, N. Mironova-Ulmane, A. I. Popov, E. Shablonin, E. Vasil'chenko, A. Lushchik, Fast-neutron-induced and as-grown

- structural defects in magnesium aluminate spinel crystals with different stoichiometry, *Optical Materials* 91 (2019) 42–49.
7. Tobias Benitez, Sergio Y. Gómez, Antonio Pedro Novaes de Oliveira, Nahum Travitzky, Dachamir Hotza, Transparent ceramic and glass-ceramic materials for armor applications, *Ceramics International* 43 (16) (2017) 13031–13046.
 8. J. M. Sands, C. G. Fountzoulas, G. A. Gilde, P. J. Patel, Modelling transparent ceramics to improve military armour, *Journal of the European Ceramic Society* 29 (2) (2009) 261–266.
 9. A. Talimian, V. Pouchly, H. F. El-Maghraby, K. Maca, D. Galusek, Transparent magnesium aluminate spinel: Effect of critical temperature in two-stage spark plasma sintering, *Journal of the European Ceramic Society* 40 (6) (2020) 2417–2425.
 10. Sagnik Das, Md Lutfor Rahman, Partha P. Mondal, Preeti L. Mahapatra, Debdulal Saha, Screen-printed MgAl_2O_4 semi-thick film based highly sensitive and stable capacitive humidity sensor, *Ceramics International*, <https://doi.org/10.1016/j.ceramint.2021.08.260>
 11. Shiva Salem, Babak Nouri, Mohammad Ghadiri, Photoactivity of magnesium aluminate under solar irradiation for treatment of wastewater contaminated by methylene blue: Effect of self-combustion factors on spinel characteristics, *Solar Energy Materials and Solar Cells* 218 (2020) 110773.
 12. Mitsunori Kitta, Toshikatsu Kojima, Riki Kataoka, Kohei Tada, Synthesis of cubic silver titanium oxide with a spinel-based structure, *Journal of Solid State Chemistry* 303 (2021) 122514.
 13. Haleh Rasouli, Mir Ghasem Hosseini, Hanieh Mashhady Kashtiban, Hierarchical FTO/PPy/ ACo_2O_4 (A: Mn or Ni) with stacks spinel structure as superb photoanodes for photoelectrochemical water splitting, *Materials Chemistry and Physics* 272 (2021) 124953.
 14. E. C. O'Quinn, J. Shamblin, B. Perlov, et al. Inversion in $\text{Mg}_{1-x}\text{Ni}_x\text{Al}_2\text{O}_4$ Spinel: New Insight into Local Structure, *Journal of American Chemical Society* 139 (30) (2017) 10395–10402.
 15. Kadhim A. M. Khalaf, Influence of the inversion factor on Madelung constants in spinel systems, *Solid State Communications* 324 (2021) 114134.
 16. R. D. Shannon, *Acta Crystallographica* A32 (1976) 751–767.
 17. Darko Kosanović, Nebojša J. Labus, Jelena Živojinović, Adriana Peleš Tadić, Vladimir A. Blagojević, Vladimir B. Pavlović, Effects of Mechanical Activation on the Formation and Sintering Kinetics of Barium Strontium Titanate Ceramics, *Science of Sintering* 52 (2020) 371–385.
 18. Nina Obradović, William G. Fahrenholtz, Suzana Filipović, Cole Corlett, Pavle Đorđević, Jelena Rogan, Predrag J. Vulić, Vladimir Buljak, Vladimir Pavlović, Characterization of MgAl_2O_4 Sintered Ceramics, *Science of Sintering* 51 (2019) 363–376.
 19. N. V. Minh, I-S. Yang, A Raman study of cation-disorder transition temperature of natural MgAl_2O_4 spinel, *Vibrational Spectroscopy* 35 (1) (2004) 93–6.
 20. R. A. Evarestov, A. Platonenko, Y. F. Zhukovskii, Site symmetry approach applied to the supercell model of MgAl_2O_4 spinel with oxygen interstitials: ab initio calculations, *Computational Materials Science* 150 (2018) 517–23.
 21. M. P. O'Horo, A. L. Frisillo, W. B. White, Lattice vibrations of MgAl_2O_4 spinel, *Journal of Physical and Chemistry of Solids* 34 (1) (1973) 23–8.
 22. M. Lazzeri, P. Thibaudeau, Ab initio Raman spectrum of the normal and disordered MgAl_2O_4 spinel, *Physical Review B* 74 (14) (2006) 140301.
 23. D. N. F. Muche, M. A. T. Marple, I. Hung, Z. Gan, R. H. R. Castro, S. Sen, Size-induced structural disorder enables ultrahard oxides, *Journal of Physical Chemistry C* 121 (2017) 13898–905.

24. Nina Obradovic, William G. Fahrenholtz, Suzana Filipovic, Smilja Markovic, Vladimir Blagojevic, Steva Levic, Slobodan Savic, Antonije Djordjevic, Vladimir Pavlovic, Formation kinetics and cation inversion in mechanically activated $MgAl_2O_4$ spinel ceramics, *Journal of Thermal Analysis and Calorimetry* 140 (2020) 95–107.
25. Vitaly Erukhimovitch, Yuval Mordekoviz, Shmuel Hayun, Spectroscopic study of ordering in non-stoichiometric magnesium aluminate spinel, *American Mineralogist* 100 (2015) 1744–1751.
26. Jonathan A. Ball, Mohsin Pirzada, Robin W. Grimes, Matthew O. Zacate, David W. Price, Blas P. Uberuaga, Predicting lattice parameter as a function of cation disorder in $MgAl_2O_4$ spinel, *Journal of Physics: Condensed Matter* 17 (2005) 7621–7631.

Сажетак: Магнезијум алуминат поседује структуру спинела и добра механичка, хемијска и термичка својства. Има широк спектар примене, укључујући рефракторну керамику, оружје и оптички транспарентна керамичка стакла. Ниска диелектрична пермеабилност и тангенс губитака пружају овој керамици примену и у електричним направама. У овом раду, прахови MgO и Al_2O_3 су помешани у моларном односу 1:1 и калцинисани на температурама између $1500^\circ C$ и $1800^\circ C$ да би се добио спинел. Након тога, узорци су смрвљени и механички активирани у млину током 60 минута да би се добио фини уситњен прах. Одређени су фазни састав, кристална структура и морфологија свих прахова. Резултати су показали да са порастом температуре расте и густина синтетисаних узорака. Млевење од 1 сата води ка формирању већих честица, али финијих прахова након млевења. XRPD и Раман спектроскопија указују на неуређену кристалну структуру након млевења.

Кључне речи: спинел, механичка активација, синтеровање, структура.

© 2023 Authors. Published by association for ETRAN Society. This article is an open access article distributed under the terms and conditions of the Creative Commons — Attribution 4.0 International license (<https://creativecommons.org/licenses/by/4.0/>).

